Improving corrosion resistance of 3D printed Ti-6Al-4V by TiN coating

Surada NISAIMUN[1], Phitsanu POOLCHARUANSIN[2], Patama VISUTTIPITUKUL[1] and Pitichon KLOMJIT[3,*]

[1] *Department of Metallurgical Engineering, Faculty of Engineering, Chulalongkorn University, 254 Payathai Rd, Patumwan, Bangkok, 10330, Thailand*

[2] *Department of Physics, Faculty of Science, Mahasarakham University, 44150, Thailand*

[3] *Rail and Modern Transportation Research Center, 114 Thailand Science Park, Pahonyothin Rd, Khlong Nueng, National Science and Technology Development Agency (NSTDA), Khlong Luang, Patumthani, 12120, Thailand*

*Corresponding author e-mail: pitichon.klo@nstda.or.th

Abstract

TiN thin films were deposited on biomaterial 3D printed Ti-6Al-4V substrates using two methods including direct current magnetron sputtering (DCMS) and high-power impulse magnetron sputtering (HiPIMS). The coating times were compared between 5 min and 25 min. HiPIMS was developed based on DCMS by increasing degree of ionization in plasma and power densities in the order of $kW \cdot cm^{-2}$ compared to $W \cdot cm^{-2}$ of DCMS. The film characteristics and mechanical properties were investigated by glancing incident x-ray diffractometer (GIXRD), field emission scanning electron microscope (FE-SEM), and atomic force microscope (AFM). Electrochemical behavior was analyzed by electrochemical impedance spectroscopy (EIS) in 1 M NaCl solution. The results showed that TiN films deposited by HiPIMS exhibited an equiaxed structure while those from DCMS had a columnar structure. As a consequence, corrosion resistance of HiPIMS films was better than the DCMS films. Furthermore, increasing coating time resulted in thicker TiN layer and therefore, promoted higher corrosion resistance.

1. Introduction

Nowadays, 3D printed Ti alloys, especially Ti-6Al-4V, as biocompatible materials have gained much interest for dental and medical applications. The 3D printing offers a nearly complete control over the manufacturing process to prepare exactly designed structures [1]. This process is favourable to produce complex-shape samples for tailored-made replacements or tooling in the medical field. To extend the biomedical applications for 3D printed Ti-6Al-4V, coating the surface was necessary to improve surface properties, e.g. hardness, wear resistance and corrosion resistance [2-6].

Titanium nitride (TiN) is a candidate material for the surface coating since it provides several superior properties, especially corrosion resistance [4-9]. Physical vapor deposition (PVD) has been reported to be a successful method for preparing TiN film on several substrates including Ti alloys. Several research groups found that by coating TiN film onto the surface, surface hardness and wear resistance can be drastically increased. However, the corrosion resistance seems to be a drawback due to a columnar structure, which is a typical structure formed by PVD coating, especially DC magnetron sputtering (DCMS). Recently, high power impulse magnetron sputtering (HiPIMS) was developed to be an alternative method for coating. The HiPIMS provides power density up to several $KW \cdot cm^{-2}$ which is significantly higher than $W \cdot cm^{-2}$ range of DCMS. HiPIMS also provides low-duty

cycle (1-10%) [10,11], extremely high power ionization sputtering with short pulse lengths (normally 100 µs), high ion flux ratio with frequency range of 10 Hz to 10 KHz. The plasma density in HiPIMS method can be achieved as high as 10^{17} to 10^{19} m^{-3} [12-14]. Therefore, film prepared by HiPIMS is expected to have high density with strong adhesion. Another unique characteristic of film prepared by HiPIMS is a non-columnar structure due to high-energy ion bombardment. With these superior characteristics, TiN film coated by HiPIMS on 3D printed Ti-6Al-4V could be a solution for low corrosion biocompatible materials. The researcher expect that the coating time affect the corrosion resistance. No one has studied the effect of coating time. Therefore, this study were compared coating time between 5 min and 25 min.

In this study, TiN thin films were coated on 3D printed Ti-6Al-4V substrates by DCMS and HiPIMS techniques to compare the film properties. The coating times for both techniques were 5 min and 25 min. The films physical properties were investigated by GIXRD, FE-SEM, AFM. The corrosion properties were investigated in 1 M NaCl solution by electrochemical impedance spectroscopy (EIS) to characterize the corrosion behavior.

2. Experimental procedure

2.1 Materials and coatings

Table 1. Coating parameters for Ti interlayer and TiN coating by DCMS and HiPIMS.

Conditions	unit	DCMS			HiPIMS		
		cleaning	Ti	TiN	cleaning	Ti	TiN
Base pressure	Torr	1×10^{-5}	-	-	1×10^{-5}	-	-
Operate pressure	mTorr	60	2.27-2.65	2.3-2.67	60	10	10
Discharge voltage	V	-1800	-300	385-396	-1800	-300	276-279
Discharge power	W	-	150	-	-	150	-
Ar flow rate	sccm	10	10	10	10	10	10
N_2 flow rate	sccm	-	-	0.5-0.6	-	-	0.2-0.3
Process time	min	10	5	5, 25	10	5	5, 25

Ti-6Al-4V specimens of 10 mm × 20 mm × 2 mm were prepared by 3D printed. The specimens were ground by silicon paper, polished with 1 µm diamond powder, and ultrasonically cleaned in acetone for 10 min. The coating process was carried out using reactive sputtering of a gas mixture of argon (99.99%) and nitrogen (99.99%). The DCMS and HiPIMS coating parameters were listed in Table 1. The coating process was started from chamber evacuation to the based pressure. After that argon gas was filled into the coating chamber until the working pressure was reached, then, the plasma was ignited. During this time, Ti film was grown on the substrate for 5 min as an interlayer, which assisted adhesion of TiN films. Nitrogen gas was introduced into the chamber to start the formation of TiN coating. Flow rates of nitrogen and argon gas were controlled by digital gas flow meters. The TiN coating process was carried out using feedback control system to avoid poisoning the target and to maintain stoichiometric TiN coating.

2.2 Film characterizations

Surface morphology and cross-sectional microstructure were determined by field emission scanning electron microscope (FE-SEM, JSM-7001F). Glancing incident X-ray diffractometer (GIXRD, D/max-2200/PC, BRUKER-D8 ADVANCE) was used to characterize the crystalline structure and phase identification of the TiN thin film using Cu K_a source, $\lambda = 1.54$ Å. Scanning rate was 0.4 degree·s^{-1}. Incident angle was 2 degree. Surface roughness of TiN coating was evaluated by atomic force microscope (AFM).

The corrosion resistance was evaluated by electrochemical impedance spectroscopy (EIS) using potentiostat (Autolab PGSTAT302N). Prior to the electrochemical testings, all samples were cleaned with deionized water. The samples were immersed in 1 M NaCl solution at room temperature during the testings. The electrochemical measurements were performed in a standard three-electrode cell with Ag/AgCl saturated in KCl as a reference electrode, a platinum rod as a counter electrode and a sample as a working electrode. The exposed area was 1 cm^2. The open circuit potential (OCP) was monitored for 60 min before all electrochemical testings. The EIS test was conducted in amplitude of 10 mV, frequency range of 10^4 to 10^{-2} Hz with data density of five frequency points per decade. EIS analysis was performed using Nova 1.11 software. The chi-squared parameters (χ^2) of the fit are in between 1×10^{-2} to 9×10^{-2}. Most of the EIS measurements were triplicated. Due to limited number of materials for testing, some conditions were replicated instead. The EIS results shown here were the representative of each condition.

3. Results and discussion

3.1 Phase identification

Figure 1 shows the X-ray diffraction patterns of Ti-6Al-4V substrate and TiN thin films prepared by DCMS and HiPIMS techniques. The diffraction pattern of the Ti-6Al-4V substrate corresponds to HCP Ti according to JCPDS No. 00-001-1198. The diffraction patterns of TiN thin films confirm the formations of FCC TiN on all coated samples. The relative intensity of TiN peak, especially (111) peak, remarkably increased with increasing coating time. This suggested that thickness of TiN significantly increased when the coating time changed from 5 min to 25 min.

To obtain the quantitative information concerning the preferential crystallite orientation, texture coefficient (*TC*) was calculated using Equation (1) below.

$$TC\,(h\,k\,l) = \frac{I_{(h\,k\,l)}/I_{r(h\,k\,l)}}{[(\frac{1}{n})\Sigma I_{(h\,k\,l)}/I_{r(h\,k\,l)}]} \tag{1}$$
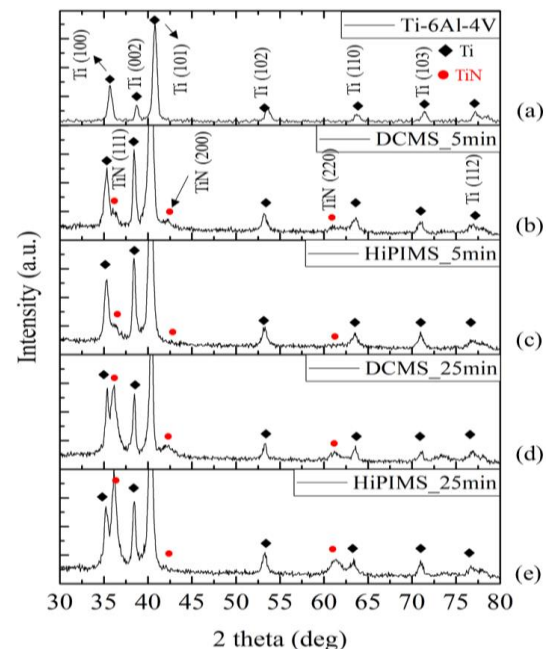
Figure 1. X-ray diffraction patterns of (a) Ti-6Al-4V substrate, TiN coating by (b) DCMS 5 min coating, (c) HiPIMS 5 min coating, (d) DCMS 25 min coating and (e) HiPIMS 25 min coating

Where $I_{(h k l)}$ is the measured relative intensity of a plane *(hkl)*. $I_{r(h k l)}$ is the standard intensity of the plane *(hkl)* taken from the JCPDS data and *n* is the number of diffraction peaks considered. The higher value of texture coefficient indicates the preferred orientation of the films along that diffraction plane [15,16]. Thus, it is expected that the adatom would be arranged into the plane with the smallest strain energy to lower the overall energy of the film [17]. The variation of *TC* for TiN coating with difference coating times and coating techniques are presented in Table 2. For 5 min coating TiN films, the *TC* values did not clearly show preferred orientation in any growth direction. For 25 min coating time, the preferred growth in 111 orientation indicates the columnar structure of TiN film in DCMS due to lowest strain energy dominated growth the preferred orientation of (111) [18]. However, HiPIMS indicates high TC value in (111) but it is not as high as in DCMS. TC value in (111) of HiPIMS is close to one in (220). Due to low strain energy in each diffraction plane, preferred growth indicates the equiaxed structure of TiN film in HiPIMS as discussed below.

3.2 Microstructures of coating

Figure 2 shows smooth surfaces of TiN films prepared by both DCMS and HiPIMS. The surfaces are without any macropore and macroparticle. Figure 3(a) and 3(c) show cross-sectional microstructure of TiN film fabricated by DCMS. The images clearly show a columnar structure, especially in the 25 min coated film. This is in good agreement with the calculated texture coefficient presented in the previous section. Figure 3(b) and 3(d) show that TiN films prepared by HiPIMS have a dense equiaxed structure without any columnar growth through the 25 min coating.

Thickness of the TiN layer is increased with increasing coating time as shown in Figure 3. The thickness values of TiN films and Ti interlayers are listed in Table 3. HiPIMS technique provides thinner TiN films than those by DCMS technique due to the sputtering effect on the film surface. The sputtering on the coating layer is a characteristic of HiPIMS due to its high-power density and high ion bombardment resulting in a thin layer. However, sputtering and ion bombardment on the film surface assist with film densification inhibiting the columnar formation and reducing the surface roughness. This significantly increases mechanical properties of the film [19]. Table 4 lists average roughness (R_a) of TiN films prepared by DCMS and HiPIMS techniques. HiPIMS technique exhibited lower R_a values than DCMS for 2 min coated TiN films as shown in Figure 4.

Table 2. Texture Coefficient (*TC*) of TiN thin films with different coating times and coating techniques.

Coating time (min)	Coating technique	Texture coefficient (TC)		
		(111)	(200)	(220)
5	DCMS	1.1478	0.6093	1.2430
	HiPIMS	1.1185	1.1349	0.7466
25	DCMS	2.0498	0.3745	0.5757
	HiPIMS	1.5716	0.2320	1.1964
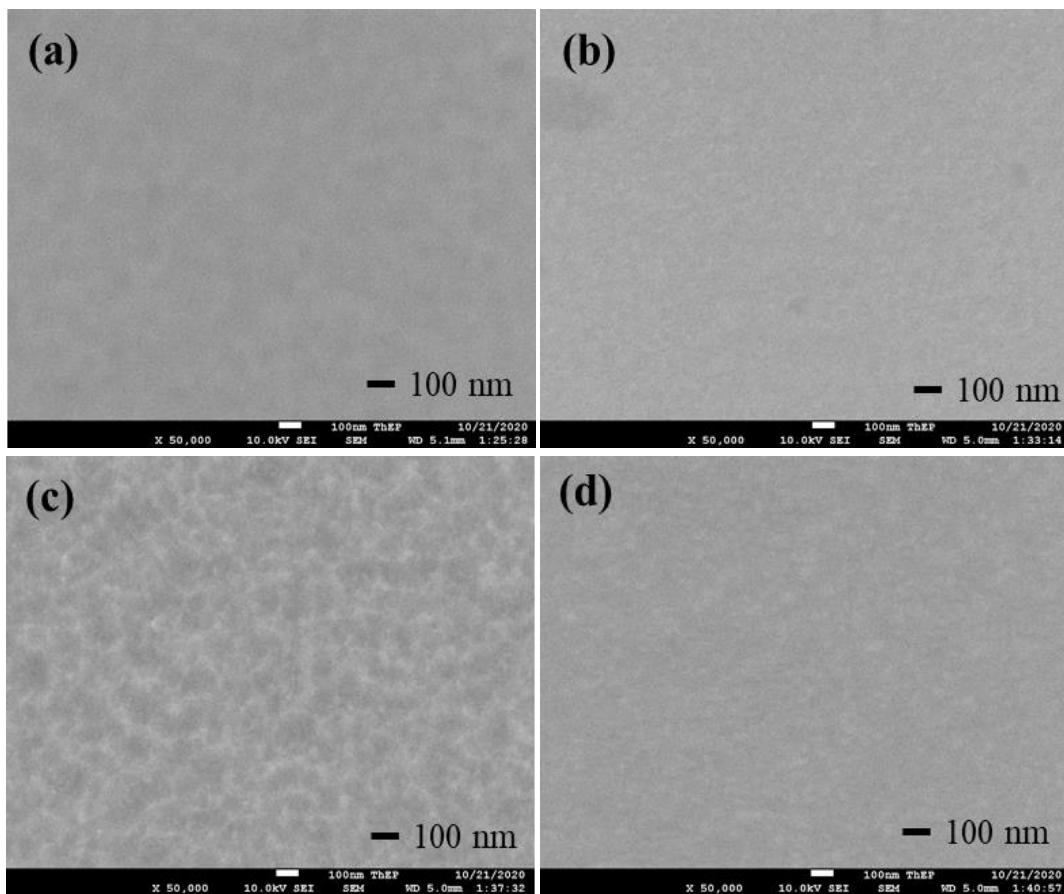
Figure 2. SEM images of TiN surface coated for 5 min by (a) DCMS, (b) HiPIMS and 25 min by (c) DCMS and (d) HiPIMS
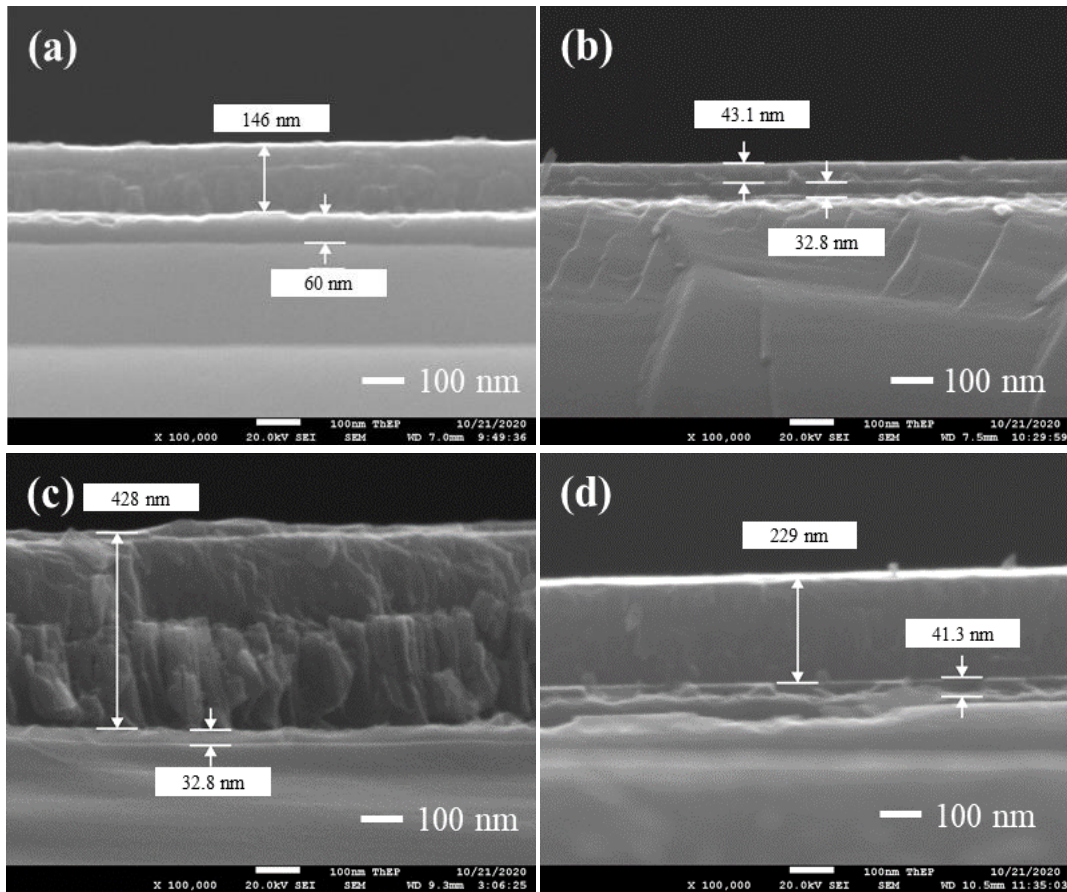
Figure 3. SEM cross-sectional microstructure of TiN films coated for 5 min by (a) DCMS, (b) HiPIMS and for 25 min, (c) DCMS and (d) HiPIMS
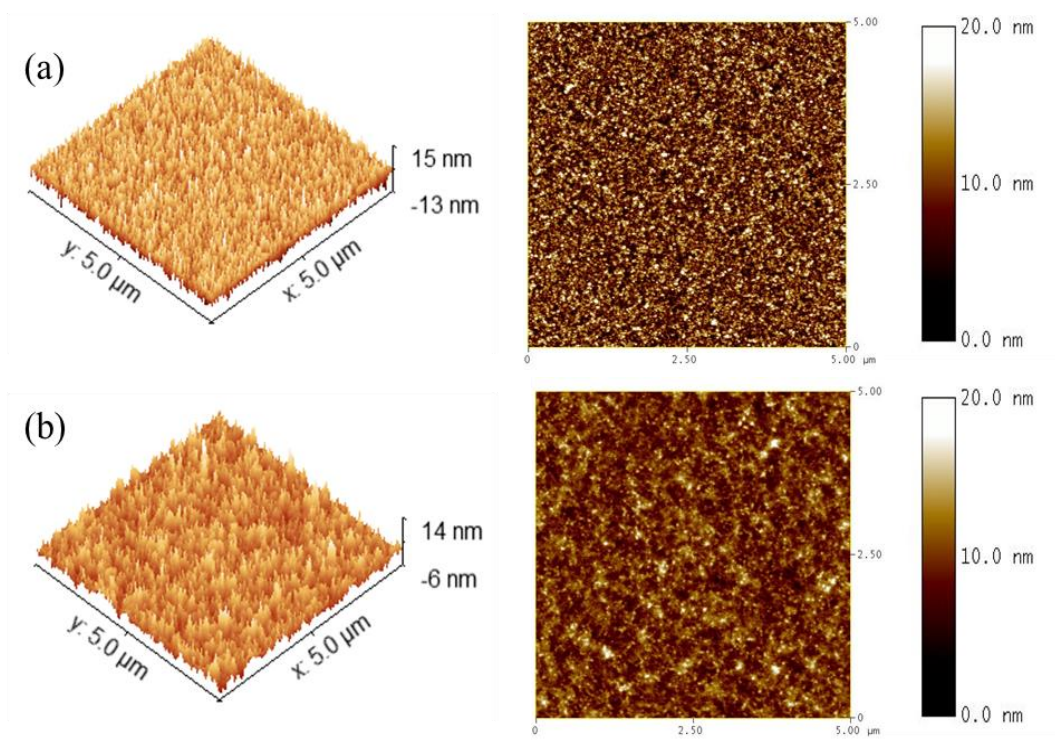

Figure 4. AFM images of surface roughness of TiN with 25 min coating time by (a) DCMS, and (b) HiPIMS

Table 3. Thickness of Ti interlayer and TiN layer by DCMS and HiPIMS

Coating time (min)	Coating technique	Thickness (nm)	
		Ti interlayer	TiN
5	DCMS	60 ± 5	146 ± 5
	HiPIMS	33 ± 5	43 ± 5
25	DCMS	33 ± 5	428 ± 5
	HiPIMS	41 ± 5	229 ± 5

Table 4. R_a values of TiN coating by DCMS and HiPIMS for 25-min coating time.

Coating techniques	R_a (nm)
DCMS	2.56
HiPIMS	1.57

3.3 Electrochemical measurement

The EIS results can be presented using both Nyquist and Bode plots. They provide information regarding interaction at the interface with minimal interruption to the surface. Both are important to characterize corrosion behavior at the interface between different surfaces.

3.3.1 Effects of coating time

The electrochemical impedance spectra of Ti-6Al-4V substrate and TiN coating samples are shown in Figure 5. The shape of the Nyquist plot is a straight line, not a semicircle. This shows that the coating film exhibits capacitive behavior [20-22]. Extrapolating to a full semicircle, the largest semicircle belongs to samples with 25 min coating time in both DCMS and HiPIMS, as shown in Figure 5(a) and 5(b). Samples with 25 min coating time showed better corrosion resistance than the ones with 5 min coating time and uncoated Ti-6Al-4V.

The Bode plots can represent the capacitive behavior of the coating. At high frequency of 10^3 to 10^4 Hz in Figure 5(c) and 5(d), the Bode modulus plot ($|Z|$) shows impedance values which correspond to electrolyte resistance (R_s) [23,24]. R_s were similar for all samples because of a fixed distance between the working electrode and the reference electrode in the experimental setup. At low frequency of 0.01 Hz, $|Z|$ values which correspond to the polarization resistance (R_p). High $|Z|$ values indicate high corrosion resistance. Coating time of 25 min in both DCMS and HiPIMS yielded higher $|Z|$ values at 0.01 Hz low frequency than 5 min coated samples and the Ti-6Al-4V substrate. Therefore, samples with 25 min coating time have the highest overall resistance.

Figure 5(e) and 5(f) show that uncoated Ti-6Al-4V substrate and TiN coated samples with 25 min coating time. in both DCMS and HiPIMS have phase angle shift remain very close to -85°. However, the TiN coated sample with 25 min coating time exhibited longer plateau region than the uncoated Ti-6Al-4V substrate. The ideal capacitor is to show phase shift at-90°. A higher level of protection is expected from TiN coat with 25 min coating time compared to 5 min coating time or uncoated Ti-6Al-4V substrate [25]. Phase angle shift were -70° and -75° for DCMS and HiPIMS for 5 min-coating time, respectively. Referring to FE-SEM coating thickness as shown in Figure 3, it indicates that samples with 25 min coating time thicker films than the 5 min coated samples both DCMS and HiPIMS. The thicker film retarded solution permeability into substrate. Both

Nyquist and Bode plots indicated that TiN with 25 min coating time had higher corrosion performance than the one with 5 min coating time.

3.3.2 Effects of coating technique

Figure 6 shows the EIS spectra of Ti-6Al-4V substrate and the TiN coated samples. For 5 min coating time, HiPIMS shows larger semicircle than DCMS and Ti-6Al-4V substrate as shown in Figure 6(a). Considering Bode modulus plot as shown in Figure 6(c), HiPIMS show higher $|Z|$ values than DCMS and Ti-6Al-4V substrate at 0.01 Hz. In Figure 6(e), phase angle shifts remain very close to -80° for HiPIMS, while phase angle shifts were very close to -70° for DCMS. Since the ideal capacitance is approach to -90°, one expects a higher level of protection or retards permeation of solution. This indicates that a highly stable passive film formed on the surface [19]. Therefore, greater phase angle shift for HiPIMS than DCMS indicated a better capacitive behavior. This implies that HiPIMS has higher corrosion protection than DCMS for 5-minute coating time.

Nyquist and Bode plots of samples with 25-minute coating time for both DCMS and HiPIMS are shown in Figure 6(b), 6(d) and 6(f). Both DCMS and HiPIMS show similar values of $|Z|$ and phase angle shift. The phase angle shifts of both coating samples remain close to -85° over a wide frequency range and exhibited plateau region that close to ideal capacitor. This indicates that TiN coating by DCMS and HiPIMS for 25 min show excellent corrosion resistance [19] due to 25 min coating time both DCMS and HiPIMS form sufficient coating thickness for protect solution permeability to substrate.

3.3.3. Equivalent electrical circuit (EC)

EIS fitting model with equivalent electrical circuit (EC) described in Figure 7, the EC depends on electrochemical and coating behaviour. The spectra from the uncoated Ti-6Al-4V substrate and 25 min coated TiN were well fitted with one time constants EC model [R(RQ)] as shown in Figure7(a) and 7(c) due to excellent coating. However, the spectra from TiN coat with 5 min coating time were fitted with two time constants EC model [R([R(RQ)]Q)] as shown in Figure 7(b) due to a very thin coating layer. The reasons why different ECs were fitted are described in the paragraph below. The EC consists of electrochemical resistance (R_s), coating resistance (R_{coat}), coating constant phase element (Q_{coat}), charge transfer resistance (R_{ct}) also known as polarization resistance (R_p) and double layer constant phase element (C_{dl}).

Constant phase element (Q or Z_{CPE}) replaces capacitance (C) in the equivalent circuit for non-ideal capacitance [1,26-29] to obtain precise fitting results. Z_{CPE} was determined by using Equation (2).

$$Z_{CPE} = \frac{1}{Y_0 (j\omega)^n} \qquad (2)$$

Giving the software values of Y_0 in unit Mho, together with a parameter know as n [30]. Where Y_0 represents the admittance magnitude of the CPE, w is radius frequency (w = 2πf), j is imaginary number ($\sqrt{-1}$), n is empirical constant [31]. Values of n is cannot over 1, n = 1 for ideal capacitor and n = 0 for resistance [14,29,32,33].
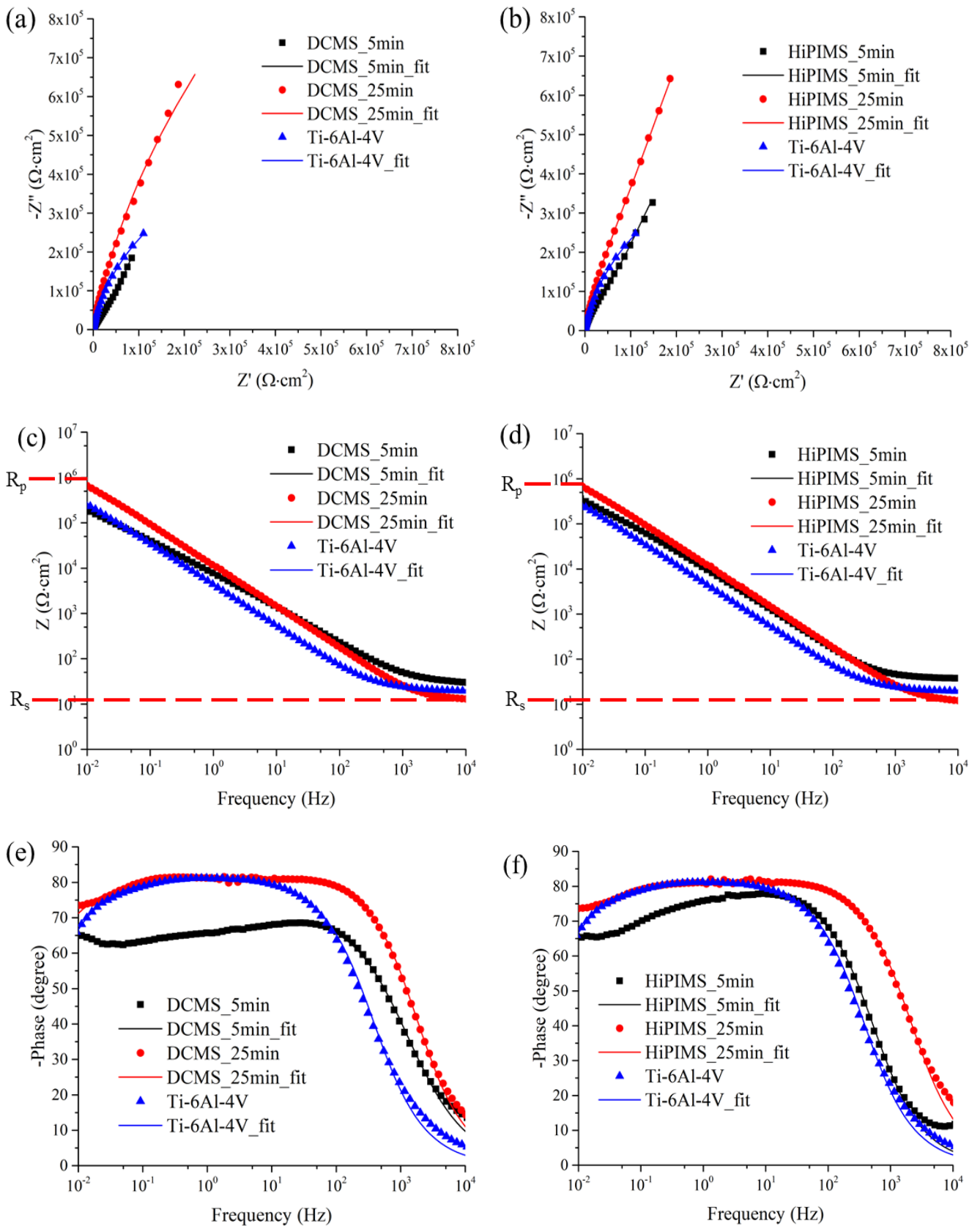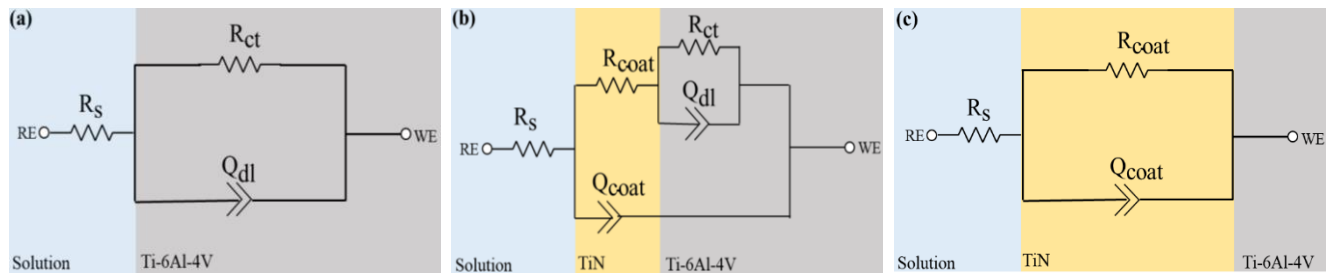
Figure 5. The electrochemical impedance spectra of TiN coated for 5 min and 25 min (a) Nyquist plot by DCMS, (b) Nyquist plot by HiPIMS, (c) Bode modulus plot by DCMS, (d) Bode modulus plot by HiPIMS, (e) Bode phase plot by DCMS, and (f) Bode phase plot by HiPIMS.
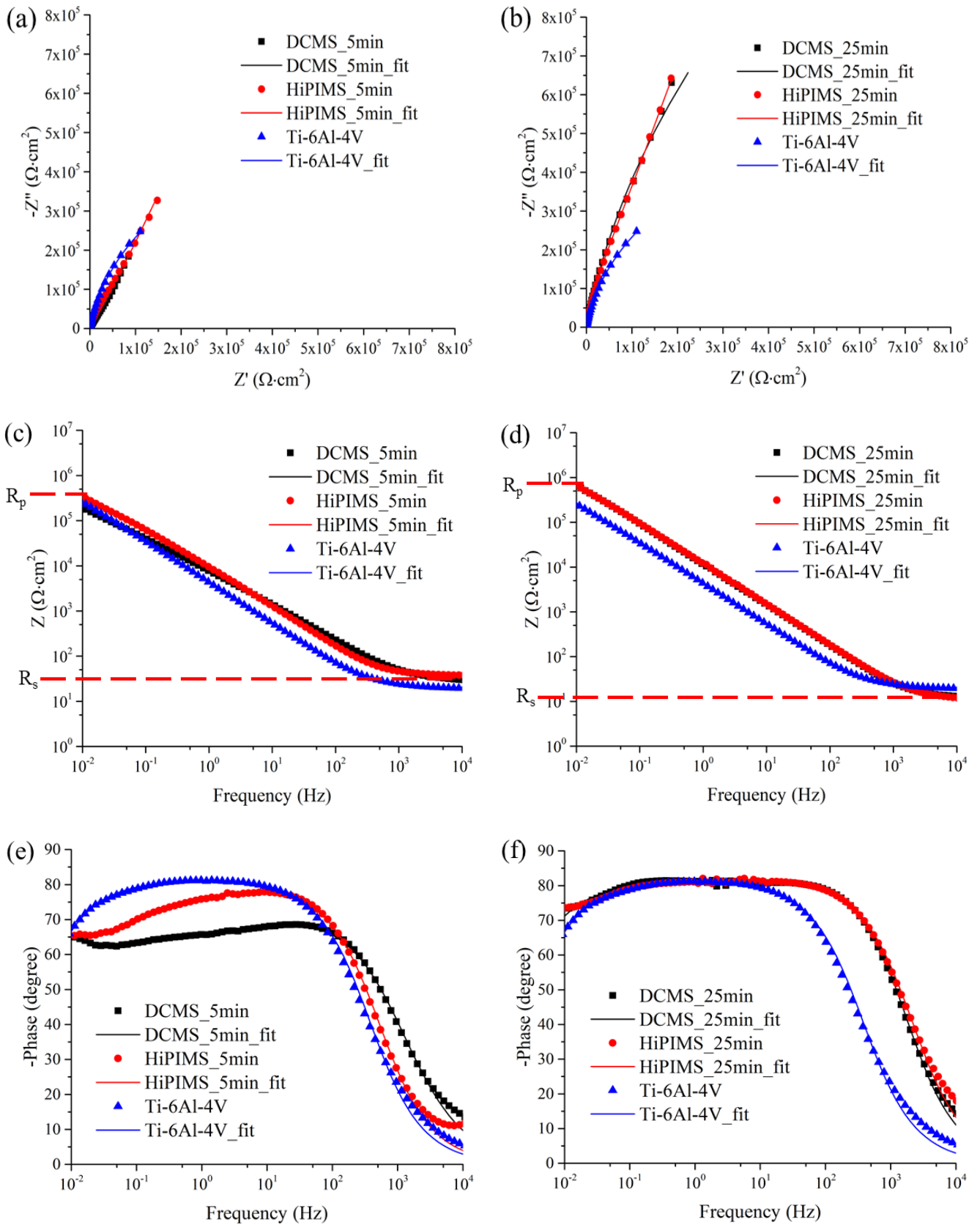
Figure 6. The electrochemical impedance spectra of TiN coating samples by DCMS and HiPIMS (a) Nyquist plot for 5 min-coating time, (b) Nyquist plot for 25 min-coating time, (c) Bode modulus plot for 5 min-coating time, (d) Bode modulus plot for 25 min-coating time, (e) Bode phase plot for 5 min-coating time, and (f) Bode phase plot for 25 min-coating time.

Table 5. Fitting EIS data obtained by equivalent electrical circuit simulation.

Coating time (min)	Samples	R_s ($\Omega \cdot cm^{-2}$)	R_{coat} ($k\Omega \cdot cm^{-2}$)	Q_{coat} Y_0 (μMho)	n	R_{ct} ($k\Omega \cdot cm^{-2}$)	Q_{dl} Y_0 (μMho)	n
0	Ti-6Al-4V	20.3	-	-	-	1,010	44.2	0.902
5	DCMS	28.1	13.3	24.1	0.81	2,580	12.7	0.587
	HiPIMS	37.4	19.6	18.7	0.90	2,610	5.93	0.521
25	DCMS	12.3	2,820	16.3	0.91	-	-	-
	HiPIMS	11.4	2,830	16.0	0.91	-	-	-

Figure 7. Equivalent electrical circuit models of samples for (a) Ti-6Al-4V substrate, TiN with (b) 5 min and (c) 25 min coating time.

As shown in Table 5, R_s is determined by the conductivity of the NaCl solution and according to these results, the solution resistance of all samples shows no significant difference [24,34].

Q_{coat} and R_{coat} are related to the coating, which can be characterized at high frequency [35-37], Q_{coat} should be a measure of solution permeation into the coating [30,38]. Y_0 and n values contribute to Q_{coat}. Typically, low Y_0 and high n values exhibit better corrosion resistant than high Y_0 and low n values. The N value approaches to 1, closely a capacitive behavior [20,22]. From Table 5, TiN coated with 25 min coating time presented lower Y_0 and higher n values than TiN coat with 5 min coating time. TiN coated with 25 min coating time improved capacitive behavior, retarded corrosion reaction at solution/coating interface better than one with 5 min coating time. R_{coat} is a measure of the defects and deterioration of the coating. R_{coat} is related to the capillary channels to the substrate surface through which the electrolyte reaches the coating/substrate interface. R_{coat} is higher because of increasing thickness and its structure. Defect-free coating layer will yield high R_{coat}. Assuming equal porosity, thicker coating will have higher R_{coat} than thinner coating. Thick coating can hinder solution diffusion through the layer. High R_{coat} in 25 min TiN coatings from both DCMS and HiPIMS were caused by increased TiN layer thickness with increasing coating time. The 25 min TiN layers were thick enough to prevent corrosion. Therefore, it well fitted with one time constant as shown in Figure 7(c). For 5 min coating time, HiPIMS indicated higher R_{coat} than DCMS. HiPIMS exhibited a dense equiaxed structure while DCMS exhibited a columnar structure. The equiaxed structure can retard penetration of solution because solution must penetrate though tortuous paths. However, solution can penetrate into the coating/substrate interfaces of both DCMS and HiPIMS for 5 min coating time due to thinner layers.

Q_{dl} and R_{ct} are related to the coating/substrate interface, which can be characterized at low frequency for 5 min coating time and the solution/substrate interface for uncoated Ti-6Al-4V substrate. 25 min coated samples do not have R_{ct} because the coating is too good. There is no charge transfer going on. That is why we fit it with one time constant. Q_{dl} can be associated with the permeability of solution into the substrate and onset of corrosion at the interface as shown in Figure 7(a) and 7(b). R_{ct} can be associated with the charge transfer resistance of the interface between coating and substrate. The higher R_{ct} and lower Y_0 values suggest a better corrosion resistance. HiPIMS had better corrosion resistance than DCMS due to coating structure as described above. Penetration of solution into the substrate for HiPIMS coating was harder than DCMS. Therefore, HiPIMS gave higher corrosion resistance than DCMS. However, Ti-6Al-4V substrate and 5 min coated TiN do not show any significant difference for corrosion resistance because thin TiN layer caused shorter path for solution to reach the substrate.

4. Conclusions

TiN films were successfully coated onto 3D printed Ti-6Al-4V substrates using DCMS and HiPIMS techniques. Film characterization shows that TiN formed by HiPIMS provides a dense equiaxed structure while the TiN formed by DCMS shows a columnar structure. Sputtering and ion bombardment happened on the HiPIMS surface resulting in a dense structure and smooth surface with low growth rate of TiN film. The EIS analysis shows one time constant from 25 min coating time can retard penetration of solution resulting in a higher R_{coat} and a lower Y_0 compared with 5 min coating time. 5 min coating time samples have two time constant. This implied that there was a penetration of solution to the interface between coating/Ti-6Al-4V substrate. Increasing coating time from 5 min to 25 min improved corrosion resistance. The equiaxed and denser structure from HiPIMS process improved corrosion resistance because it retarded penetration of solution through the coating while the columnar structure from DCMS was easier for solution to permeate into coating/substrate interface. Moreover, DCMS required a certain coating thickness to resist corrosion while a thin layer from HiPIMS could do so. In this study, minimum required thickness for DCMS was about 400 nm from the 25 min coated sample.

Acknowledgements

References

[1] X. Z. Jie Jin, and H. Liu, "Duration and degradation of CrMoN coated SS316L in simulated PEMFCs environment: High potential polarization and electrochemical impedance spectroscopy (EIS)," *International Journal of Hydrogen Energy,* vol. 44, pp. 20293-20303, 2019.

[2] A. M. G. Ortiz-de-Zarate, A. Garay, L. Azpitarte, I. Sacristan, M. Cuesta, and P. J. Arrazola, "Experimental and FEM analysis of surface integrity when broaching Ti64," vol. 71, pp. 466-471, 2018.

[3] A. T. Sidambe, "Biocompatibility of Advanced Manufactured Titanium Implants-A Review," *Materials (Basel),* vol. 7(12), pp. 8168-8188, 2014.

[4] W-Y Wua, and M.-Y. C., Y-H. Hsua, G-Z. Chena, S-C. Liaoc, C-H. Leed, and P-W. Luie, "Bioapplication of TiN thin films deposited using high power impulse magnetron sputtering," *Surface & Coatings Technology,* vol. 362, pp. 167-175, 2019.

[5] A. Scerri, J. Buhagiar, S. Bandield, J. C. Avelar-Batista Wilson, J. Housden, A. Leyland, A. Matthews, and G. Cassar, "Corrosion behaviour of triode plasma diffusion treated and PVD TiN-coated Ti–6Al–4V in acidified aqueous chloride environments," *Surface and Coatings Technology,* vol. 280, pp. 185-193, 2015.

[6] J. Paulitsch, M. Schemkel, Th. ZufraB, P. H. Mayrhofer, and W.-D. Munz, "Structure and properties of high power impulse magnetron sputtering and DC magnetron sputtering CrN and TiN films deposited in an industrial scale unit," *Thin solid film,* vol. 518(19), pp. 5558-5564, 2010.

[7] X. Zhao, H. Liu, S. Li, X. Wang, Y. Sheng, P. Zhang, and W. Li, "Combined effect of TiN coating and surface texture on corrosion-wear behavior of selective laser melted CP-titanium in simulated body fluid," *Journal of Alloys and Compounds,* vol. 816, 2020.

[8] F. M. Kgoete, A. P. I. Popoola, and O. S. I. Fayomi, "Data on the influence of TiN on wear and corrosion behavior of Ti–6Al–4V alloy fabricated," *Data in Brief,* vol. 19, pp. 1989-1996, 2018.

[9] M. Husseina, N. K. Ankaha, A. M. Kumara, M. Azeemb, S. Saravanan, A. Soroura, and N. Aqeelib, "Mechanical, biocorrosion, and antibacterial properties of nanocrystalline TiN coating for orthopedic applications," *Ceramics International,* vol. 46, pp. 18573-18583, 2020.

[10] A. Ferrec, J. Keraudy, S. Jacq, F. Schuster, P.-Y. Jouan, and M. A. Djouadi, "Correlation between mass-spectrometer measurements and thin film characteristics using dcMS and HiPIMS discharges," *Surface and Coatings Technology,* vol. 250, pp. 52-56, 2014.

[11] D. Lundin, and K. Sarakinos, "An introduction to thin film processing using high-power impulse magnetron sputtering," *Journal of Materials Research*, vol. 27(5), pp. 780-792, 2012.

[12] A. Sudip, M. M. O. Ashraf, S. Adhikari, M. Rusop, H. Uchida, and M. Umeno "Diamond-like carbon thin films grown by large-area surface-wave mode microwave plasma CVD: Effects of stage distance to microwave window," *Diamond and Related Materials,* vol. 15(4-8), pp. 913-916, 2006.

[13] U. Helmersson, M. Lattemann, J. Bohlmark, A. P. Ehiasarian, and J. T. Gudmundsson, "Ionized physical vapor deposition (IPVD): A review of technology and applications," *Thin Solid Films,* vol. 513(1-2), pp. 1-24, 2006.

[14] Z. He, S. Zhang, and D. Sun, "Effect of bias on structure mechanical properties and corrosion resistance of TiNx films prepared by ion source assisted magnetron sputtering " *Thin Solid Films,* vol. 676, pp. 60-67, 2019.

[15] S. Girjesh, S. B Shrivastava, D. Jain, S. Pandya, T. Shripathi, and V. Ganesan "Effect of indium doping on zinc oxide films prepared by chemical spray pyrolysis technique," *Bulletin of Materials Science*, vol. 33(5), pp. 581-587, 2010.

[16] T. Prasada Rao, and M. C. Santhoshkumar, "Highly oriented (1 0 0) ZnO thin films by spray pyrolysis," *Applied Surface Science,* vol. 255(16), pp. 7212-7215, 2009.

[17] U. C. Oh, and J. Ho Je "Effects of strain energy on the preferred orientation of TiN thin films," *Journal of Applied Physics,* vol. 74(3), pp. 1692-1696, 1993.

[18] M. Caglar, S. IIican, Y. Caglar, and F. Yakuphanoglu, "Electrical conductivity and optical properties of ZnO nanostructured thin film," *Applied Surface Science* vol. 255(8) pp. 4491-4496, 2009.

[19] E. Hasan, A. Faridreza, F-A. Arash, and K. H. Kim, "Microstructural and electrochemical comparison between TiN coatings deposited through HiPIMS and DCMS techniques," *journal of Alloys and Compounds,* vol. 735, pp. 422-229, 2018.

[20] P. Canepa, G. Ghiara, R. Spotorno, M. Canepa, and O. Cavalleri, "Structural vs. electrochemical investigation of niobium oxide layers anodically grown in a Ca and P containing electrolyte," *Journal of Alloys and Compounds,* vol. 851, pp. 156937, 2021.

[21] X. Zhao, D. Yan, S. Li, and C. Lu, "The effect of heat treatment on the electrochemical corrosion behavior of reactive plasma-sprayed TiN coatings," *Applied Surface Science,* vol. 257(23), pp. 10078-10083, 2011.

[22] D. A. Jones, *Principles and prevention of corrosion*. Pearson, 1996.

[23] J. Jin, X. Zhao, and H. Liu, "Durability and degradation of CrMoN coated SS316L in simulated PEMFCs environment: High potential polarization and electrochemical impedance spectroscopy (EIS)," *International Journal of Hydrogen Energy,* vol. 44(36), pp. 20293-20303, 2019.

[24] D. Turcio-Ortega, S. E. Rodil, and S. Muhl, "Corrosion behavior of amorphous carbon deposit in 0.89% NaCl by electrochemical impedance spectroscopy," *Diamond and Related Materials,* vol. 18(11), pp. 1360-1368, 2009.

[25] R. G Kelly, J. R Scully, D. W Shoesmith, and R. G Buchheit, "Electrochemical Techniques in Corrosion Science and Engineering,", CRC Press, 2003.

[26] C. Liu, Q. Bi, A. Leyland, and A. Matthews, "An electrochemical impedance spectroscopy study of the corrosion behaviour of PVD coated steels in 0.5 N NaCl aqueous solution: Part I. Establishment of equivalent circuits for EIS data modelling," *Corrosion Science,* vol. 45(6), pp. 1243-1256, 2003.

[27] H. Cesiulis, N. Tsyntsaru, A. Ramanavicius, and G. Ragoisha, "Chapter 1 The study of Thin Films by Electrochemical Impedance Spectroscopy," in Nanostructures and Thin Films for Multifunctional Applications, Springer International Publishing, Ion Tiginyanu, Pavel Topala, Veaceslav Ursaki, pp. 3-34, 2016.

[28] Z. He, S. Znang, and D. Suna, "Effect of bias on structure mechanical properties and corrosion resistance of TiN_x films prepared by ion source assisted magnetron sputterin," *Thin Solid Films,* vol. 676, pp. 60-67, 2019.

[29] S. H. Ahn, J. H. Hong, J. G. Kim, and J. G. Han, "Effect of microstructure on corrosion behavior of TiN hard coatings produced by a modified two-grid attachment magnetron sputtering process," *Thin Solid Films,* vol. 515(17), pp. 6878-6883, 2007.

[30] J. Molina, M. Puig, M. J. Gimeno, R. Izquierdo, J. J. Gracenea, and J. Suay, "Influence of zinc molybdenum phosphate pigment on coatings performance studied by electrochemical methods," *Progress in Organic Coatings,* vol. 97, pp. 244-253, 2016.

[31] G. M. Tavarez-Martinez, E. Onofre-Bustamante, E. C. De La Cruz-Terrazas, M. I. Escudero-Rincon, and M. A. Dominguez-Crespo, "Evaluation of TiO_2/CeO_2 coating on Ti6Al4V alloy in PBS physiological medium using conventional and near field electrochemical techniques," *Applied Surface Science,* vol. 494, pp. 1109-1118, 2019.

[32] A. Döner, and G. Kardaş, "N-Aminorhodanine as an effective corrosion inhibitor for mild steel in 0.5M H2SO4," *Corrosion Science,* vol. 53(12), pp. 4223-4232, 2011.

[33] E. Machnikova, K. H. Whitmire, and N. Hackerman, "Corrosion inhibition of carbon steel in hydrochloric acid by furan derivatives," *Electrochimica Acta,* vol. 53(20), pp. 6024-6032, 2008.

[34] S. H. Mosavat, M. H. Shariat, and M. E. Bahrololoom, "Study of corrosion performance of electrodeposited nanocrystalline Zn-Ni alloy coatings," *Corrosion Science,* vol. 59, pp. 81-87, 2012.

[35] M. J. Gimeno, M. Puig, S. Chamorro, J. Molina, R. March, E. Oró, P. Pérez, J. J. Gracenea, and J. Suay, "Improvement of the anticorrosive properties of an alkyd coating with zinc phosphate pigments assessed by NSS and ACET," *Progress in Organic Coatings,* vol. 95, pp. 46-53, 2016.

[36] S. Ghasemi, A. Shanaghi, and P. K. Chu, "Corrosion behavior of reactive sputtered Ti/TiN nanostructured coating and effects of intermediate titanium layer on self-healing properties," *Surface and Coatings Technology,* vol. 326, pp. 156-164, 2017.

[37] C. Liu, Q. Bi, and A. Matthews, "EIS comparision on corrosion performance of PVD TiN and CrN coated mild steel in 0.5 N NaCl aqueous solution," *Corrosion Science,* vol. 43(10), pp. 1953-1961, 2001.

[38] M. J. Gimeno, S. Chamorro, R. March, E. Oro, P. Perez, J. J. Gracenea, and J. Suay, "Anticorrosive properties enhancement by means of phosphate pigments in an epoxy 2k coating. Assessment by NSS and ACET," *Progress in Organic Coatings,* vol. 77(12), pp. 1993-1999, 2014.